Clays and Clay Minerals, Vol. 52, No. 4, 432–442, 2004.

ON THE MECHANISMS OF APOPHYLLITE ALTERATION IN AQUEOUS SOLUTIONS. A COMBINED AFM, XPS AND MAS NMR STUDY

KIRILL ALDUSHIN[1,2], GUNTRAM JORDAN[1,*], MICHAEL FECHTELKORD[1], WOLFGANG W. SCHMAHL[1], HANS-WERNER BECKER[3] AND WERNER RAMMENSEE[2]

[1] Institut für Geologie, Mineralogie und Geophysik, Ruhr-Universität Bochum, 44780 Bochum, Germany
[2] Institut für Mineralogie und Geochemie, Universität zu Köln, Zülpicher Str. 49b, 50674 Köln, Germany
[3] Institut für Physik mit Ionenstrahlung (Exp. Physik III), Ruhr-Universität Bochum, 44780 Bochum, Germany

Abstract—Apophyllite, a hydrous K-Ca-phyllosilicate, reacts with acidic aqueous solutions at room temperature. Various analytical methods have been applied to study the mechanism of the reaction and its characteristics, *i.e.* the changes in chemical composition, modifications in crystal structure and alterations in surface morphology. In contact with acidic solution, protonation of the terminal, non-bridging oxygen at the silicate tetrahedra takes place and the interlayer cations K^+ and Ca^{2+} are removed. The protonation and ion removal causes the interlayer spacing to increase. Atomic force microscopy shows that the increase takes place discontinuously and, therefore, reflects a discontinuous reaction that comprises a two- or three-step protonation. Additionally, three structurally different protonation sites have been detected by nuclear magnetic resonance spectroscopy which also differ in the amount of close-by hydrogen, although in pristine apophyllite all terminal oxygen positions at silicate tetrahedra are structurally equivalent. In many clay minerals such structurally different protonation sites have not been detected so far. Thus, the multi-step protonation process in apophyllite clearly demonstrates the vast sensitivity of the protonation reaction on small structural variations in phyllosilicates.

Key Words—Acidic Leaching, Apophyllite, Atomic Force Microscopy, Cation Exchange, Crystalline Silicic Acid, Dissolution, Nuclear Magnetic Resonance Spectroscopy, Phyllosilicates, Surface Alteration, Swelling.

INTRODUCTION

Detailed studies of reactions of phyllosilicates with acidic solutions provide insight into fundamental natural processes, such as weathering, formation of minerals, or geochemical cycling (*e.g.* Nagy *et al.*, 1991; Wieland and Stumm, 1992; Walther, 1996). These investigations are also important for industrial applications, *e.g.* production of sorbents, catalyst carriers, decontaminants (Corma and Perez-Pariente, 1987; Ravichandran and Sivasankar, 1997; Saito *et al.*, 1997; Temuujin *et al.*, 2001). The reactions with acidic solutions cause a selective leaching of cations located in the octahedral sheet of phyllosilicates and, in some cases, lead to the formation of an amorphous phase or at least to a significant loss of crystallinity of the product (Frondel, 1979; Kaviratna and Pinnavaia, 1994; Aznar *et al.*, 1996). In other cases, cation depletion does not cause decomposition of the structure and the product retains the structural features of the parental mineral (Lagaly *et al.*, 1975; Frondel, 1979; Pabst, 1958; Rodriguez *et al.*, 1994; Kosuge *et al.*, 1995). Generally, phyllosilicate reactions in acidic solution have been studied by X-ray diffraction (XRD), magic angle spinning nuclear magnetic spectroscopy (MAS NMR), infrared (IR) spectroscopy and BET surface area analysis. Morphological changes have typically been studied *ex situ* by scanning electron microscopy (SEM) and *in situ* by atomic force microscopy (AFM). Atomic force microscopy is known as a powerful method for the *in situ* investigation of surface-liquid interfaces and has successfully been applied to the investigation of various alteration processes on mineral surfaces as well as to crystal growth and dissolution (*e.g.* Shiraki *et al.*, 2000; Teng *et al.*, 2001; Astilleros *et al.*, 2002; Deuster *et al.*, 2003; Duckworth and Martin, 2003; Peskleway *et al.*, 2003), even under hydrothermal conditions (Jordan *et al.*, 1999; Higgins *et al.*, 2002; Aldushin *et al.*, 2004). Studies by AFM on the behavior of phyllosilicates in acidic solution have been performed by *e.g.* Bosbach *et al.* (2000), Bickmore *et al.* (2001), Brandt *et al.* (2003), Liu *et al.* (2003) and Aldushin *et al.* (2004).

Apophyllite [$KCa_4Si_8O_{20}(F,OH)\cdot 8H_2O$] is a hydrous sheet silicate. Its structure is tetragonal (*P*4/*mnc*, a = 8.96 Å, c = 15.8 Å; Colville *et al.*, 1971). Perpendicular to the c axis, layers composed of silicate tetrahedra alternate with layers of Ca, K, F and OH (Figure 1). The silicate layers of apophyllite are composed of interconnected four- and eight-membered rings, with the terminal, non-bridging tetrahedra apices of the four-membered rings alternately pointing up and down along the c direction. The terminal apices of adjoining layers oppose each other and form a ≡Si–O–Ca–O-Si≡ type bonding via Ca^{2+}, thus forming a kind of a framework with alternating voids. Apophyllite, therefore, has many

* E-mail address of corresponding author:
guntram.jordan@ruhr-uni-bochum.de
DOI: 10.1346/CCMN.2004.0520404

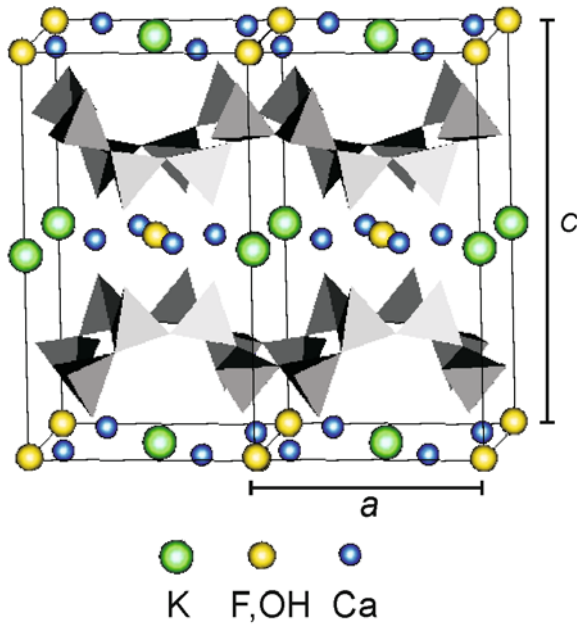

Figure 1. Structure of apophyllite: four- and eight-member silicate-rings in (001), with 4-member rings alternately pointing up and down; planes of cations, hydroxyls and fluorine ions alternate with silica layers. H_2O molecules have been omitted for clarity. The image was created using *xtal-3D*.

structural similarities not only to important sheet silicates, particularly clays, but also to silicates with structural voids or cages like zeolites. The investigation of the kinetics and mechanism of reactions of apophyllite in aqueous solutions can, therefore, give useful insights into the alteration processes of other silicates.

The formation of a crystalline residue of apophyllite caused by acidic solution has been reported by several authors (Frondel, 1979; Lagaly and Matouschek, 1980; Sogo *et al.*, 1998). Frondel (1979) reported the formation of a crystalline silica hydrate (Silica-AP, $H_2Si_4O_9$) by the decomposition of apophyllite in acidic solution (HCl) at room temperature. Lagaly and Matouschek (1980) observed the formation of H-apophyllite ($H_8Si_8O_{20}{\cdot}xH_2O$) after the treatment of apophyllite in acidic solution at 0–4ºC. According to these authors, both hydrates maintain the structure of apophyllite silica layers. In addition to the XRD experiments in these studies, batch experiments performed by Cave (2002) show that apophyllite dissolves non-stoichiometrically in acidic solution with a preferential loss of interlayer cations.

In previous work, Aldushin *et al.* (2004) investigated the kinetics of the alteration of apophyllite (001) surface in aqueous solutions by hydrothermal AFM (HAFM) and Rutherford backscattering spectroscopy (RBS). It was shown that square-shaped hillocks cover the surface at low pH (see Figure 2). The hillocks are softer than the pristine surface, 3–4 Å high, and spread laterally on the surface. The activation energy for the spreading of the hillocks was found to be 58±4 kJ/mol. The hillock formation was described as a penetration of hydronium ions into the interlayer region, forming silanol groups at the silicate tetrahedrons, and initiating the release of K, Ca and F. Since the silicate layers of apophyllite are linked by Ca^{2+} ions, their release causes a reduction of bonding strength between the silicate layers. This in turn causes an increase in interlayer distance. The same reaction also proceeds in successive layers causing the formation of several generations of hillocks; the hillocks of younger generation are apparently above older hillocks. The reaction can be summarized as a proton-promoted ion-replacement reaction which proceeds layer by layer beneath the surface into the bulk crystal (Aldushin *et al.*, 2004).

In the present study we combine *in situ* AFM investigations of the surface reaction of apophyllite in aqueous solution with MAS NMR and XPS spectroscopy. This approach allows us to yield detailed information about the mechanisms of the transformation of apophyllite into a crystalline silicic acid due to its interaction with acidic aqueous solutions.

EXPERIMENTAL

In all experiments, natural, transparent and colorless fluorapophyllite crystals (Poona, India; for microprobe analysis see Aldushin *et al.*, 2004) were used. The crystals were cleaved by a knife immediately before they were affixed in the fluid cell by a titanium wire and immersed in solution. The samples used were 0.2–1.5 mm thick and the size of the (001) surface was ~5–15 mm^2. The duration of the experiments was up to 15 h.

Solutions were prepared using high-purity deionized water (resistivity: 18 MΩ cm). The pH values of solutions were adjusted to 1.5–3 by adding HNO_3 and to 9–12 by adding NaOH. The solutions were prepared without adding any further background electrolyte. The flow rate of the solution through the fluid cell was set to values between 0 and 14 µL/s.

All *in situ* measurements were carried out using a contact-mode hydrothermal atomic force microscope (HAFM) which was constructed in our laboratories. Although this device enables *in situ* measurements of the solid-liquid interface at pressures up to 50 bar and temperatures up to 170ºC, the experiments presented here were performed at room temperature and ambient pressure exclusively. All AFM images are presented in 'deflection mode' (Veeco Instruments) and may be perceived as morphological images illuminated from the left. Uncoated Si cantilevers with integrated tips (spring constant: 0.1–0.3 N/m) were used.

X-ray photoelectron spectroscopy (XPS) was conducted to analyze the chemical composition of the near-surface region of the apophyllite (001) surface after the crystals had been reacted in acidic solution. For the measurements we used freshly cleaved apophyllite crystals which were immersed in HNO_3 solutions at

https://doi.org/10.1346/CCMN.2004.0520404 Published online by Cambridge University Press

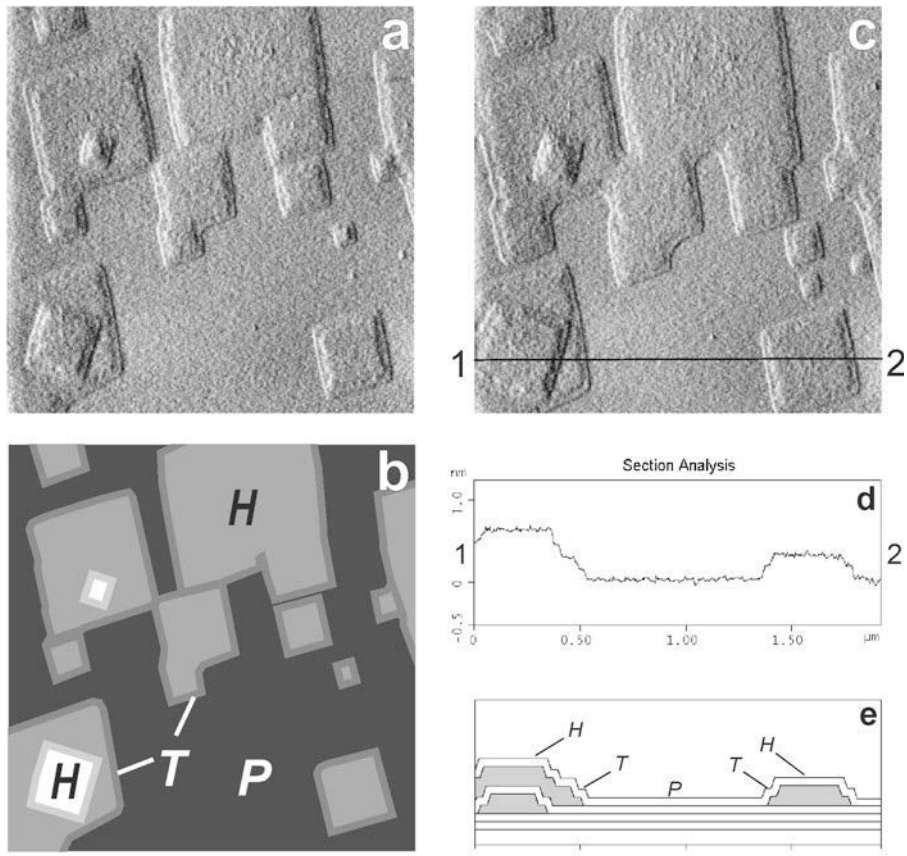

Figure 2. (a) Formation of hillocks on the (001) pristine apophyllite surface (area *P*) at pH 2.5. Mature hillocks (area *H*) are surrounded by lower terraces (area *T*). In the left side of the image a second generation of hillocks can be observed (scan field 2 µm × 2 µm, all AFM images are presented in 'deflection mode' and may be perceived as morphological images illuminated from the left); (b) schematic image of (a) showing the different areas in different grayscales; (c) 8 min later: the hillocks coalesce first by merging of the lower terrace (*T*) and then by merging of the main hillocks (*H*); (d) cross-section as labeled in (c); (e) schematic model based on the cross-section showing the actual location of swelling interlayers, colorless stripes: silicate layers, gray regions: protonated interlayers.

pH 2.5 for 1, 3 and 5 h. After the treatment, the crystals were air dried for 30 min and mounted into the spectrometer together with a freshly cleaved, untreated sample as a reference.

The measurements were performed in a surface analysis VG/Fisons system which is equipped with a CLAM2 analyzer. The base pressure in the system is 5×10^{-9} mbar. During measurements, samples were oriented at 45º with respect to the X-ray gun as well as to the analyzer. The AlKα line was used for the emission of the photoelectrons, which were analyzed with a pass energy of 100 eV. A survey spectrum was taken from each sample as well as more detailed spectra of the regions of interest.

For NMR analysis, apophyllite crystals were ground in a mortar and immersed into HNO_3 solutions at pH 1−2.5 (initial pH) for 1−11 h. The increase in pH of the solution by the progressing reaction was kept within one pH unit by choosing appropriate solution to sample ratios. The NMR spectra were recorded on a Bruker ASX 400 NMR spectrometer at a magnetic field strength of 9.34 T. The ^{29}Si MAS NMR measurements were carried out at 79.49 MHz using a standard Bruker 7 mm MAS probe with a sample spinning rate of 3.5 kHz, a single pulse duration of 2 µs (90º pulse length 5.8 µs) and 1000−1600 scans were accumulated with a 60 s recycle delay. The $\{^1H\}$ ^{29}Si CPMAS NMR experiments were carried out with a ^{1}H 90º pulse length of 9.0 µs and contact times of 250 µs, 1.0 ms and 3.0 ms. Shifts were referenced to tetramethylsilane for ^{1}H and ^{29}Si. The ^{1}H MAS NMR spectra were obtained at 400.13 MHz using a standard Bruker 4 mm MAS probe. Typical conditions were pulse lengths of 2.0 µs pulse length (90 degree pulse length 5.0 µs) and a 60 s recycle delay. 32 scans were accumulated at a MAS rotation frequency of 12 kHz for the ^{1}H MAS NMR spectra.

RESULTS

Atomic force microscopy

Figure 2a shows hillocks developing on the pristine (001) surface of apophyllite due to the interaction with

https://doi.org/10.1346/CCMN.2004.0520404 Published online by Cambridge University Press

acidic solution (pristine surface = area *P* on the scheme in Figure 2b). A thorough examination of the morphology of the hillocks reveals that they are not uniform in height but can be differentiated into a lower surrounding terrace (area *T*) and the higher, main hillock (area *H*). This can also be seen on Figure 2d, showing a cross section of the line indicated on Figure 2c. The height of the terrace is 1.5±0.5 Å whereas the height of the main hillock is 3.5±0.5 Å. The terrace width reaches values of up to 25 nm. Based on the cross-section in Figure 2d, Figure 2e shows a schematic model representing the locations of excess thickness in the apophyllite sheet structure. The step between the pristine surface (*P*) and the terrace (*T*) is straight, whereas the step between the terrace (*T*) and the main hillock (*H*) is jagged. Entire hillocks (*T* + *H*) are spreading laterally, coalescing, and forming a uniform layer (Figure 2c). The coalescence first takes place by merging of the lower terrace (*T*) and then by merging of the main hillocks (*H*).

However, there is not just a single mechanism of hillock merger. Figure 3a shows two merging hillocks. After the coalescence of the terraces (*T*) of the two hillocks (Figure 3b), the combined area *T* separates from the inner corner and moves away from the main hillocks (*H*). The separating area *T* forms a bridge-like conjunction (marked by an arrow on Figure 3b) between the two hillocks. This conjunction moves rapidly leaving behind an apparently unaltered surface area (*A*) with a height similar to the pristine surface. The rapid movement of the conjunction stops when the position parallel to the hillock orientation has been reached, thus enveloping the two merging hillocks (Figure 3c–e). Upon ceasing rapid movement and acquiring the enveloping position, the conjunction begins to swell (*i.e.* to transform into state *H*) and to develop its own surrounding terrace at its outer perimeter (area *T*). Then, the conjunction begins to spread laterally slowly (Figure 3f). In the case of a merger with another hillock, the surrounding terrace can again separate and form a new conjunction. However, at the inner perimeter of a conjunction, which has been transformed into state *H*, no new surrounding terrace develops. This clearly indicates that the area *A*, through which the rapidly moving conjunction has passed, behaves differently from the pristine surface (area *P*).

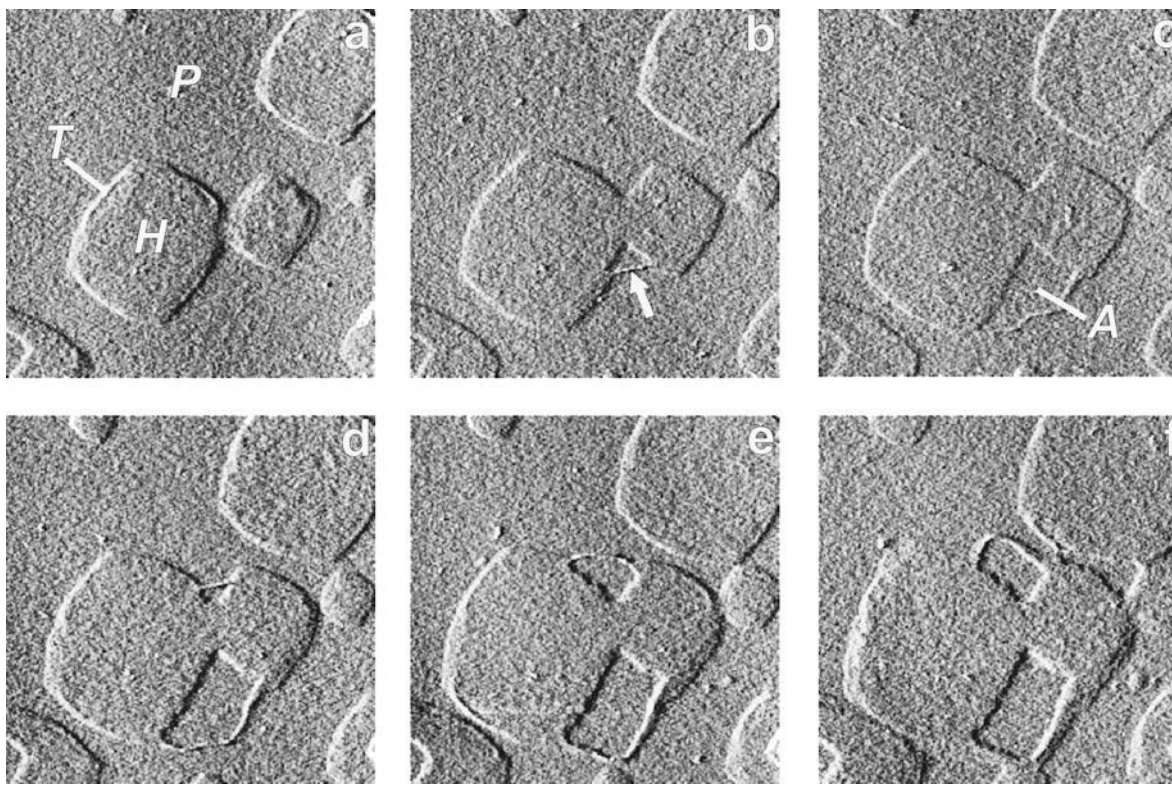

Figure 3. Formation of conjunctions between two hillocks at pH 2.5 (image acquisition for parts b, c, d, e, f at 6, 9, 12, 15 and 20 min after a, respectively). (a) Two merging hillocks; pristine surface *P*, lower terraces *T* and mature hillocks *H* can be observed; (b) in the lower inner corner of the hillocks, the combined terrace separates from the mature hillocks forming a conjunction (marked by an arrow) between the hillocks; (c–e) the conjunction moves rapidly, leaving behind an apparently unaltered surface area (*A*); a second conjunction forms in the upper inner corner between the hillocks; (f) the conjunctions stop moving when the position parallel to the hillock step orientation has been reached. The conjunctions now begin to widen in lateral dimension and develop a surrounding terrace at the outer perimeter. Scan field 0.9 μm × 0.9 μm.

https://doi.org/10.1346/CCMN.2004.0520404 Published online by Cambridge University Press

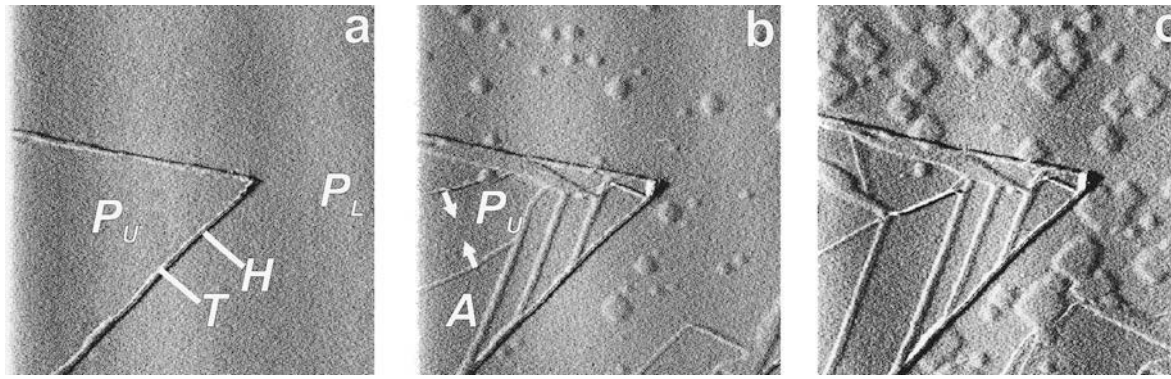

Figure 4. Formation of conjunctions at cleavage steps (pH 2): (a) from right to left: pristine lower layer (state P_L), mature hillock on upper layer (state *H*), upper layer in state *T*, pristine upper layer (state P_U); (b) 11 min later: parallel pattern of mature stripes of state *H*; two conjunctions (marked by arrows) can be seen approaching each other; (c) 10 min later: the two conjunctions have coalesced and stopped moving. Since on both sides of the united conjunction, area *A* has been formed, no new conjunction can emanate from this stripe. Scan field 2.7 μm × 2.7 μm.

The direct transition of area *A* into a mature hillock (state of area *H*) was found to be 7–10 times slower than the transformation of the pristine surface (*P*) into state *H* via state *T*. The step at the transition $A \rightarrow H$ is jagged and in some cases has a branched or dendrite-like shape. Furthermore, within area *A* subsequent hillock formation is impeded even within lower layers (beneath the areas transformed to state *A*).

The formation of conjunctions can also be observed at cleavage steps (Figure 4). The reaction initiates at the edges of the step forming a uniform sequence of states across the step (Figure 4a; from right to left): pristine lower layer (state P_L) → mature hillock on upper layer (state *H*) → upper layer in state *T* → pristine upper layer (state P_U). Then, on the upper layer, state *T* separates and rapidly moves away from state *H* leaving behind an area in state *A* (Figure 4b). As in the case of conjunctions at merging hillocks, new conjunctions can separate from the conjunction which has stopped moving and has differentiated into state *T* and *H*. In this way, the parallel pattern of mature stripes of state *H* (Figure 4b,c) is caused by a sequence of conjunctions which are separating, moving, stopping and differentiating. Additionally, in Figure 4b two conjunctions can be seen approaching each other. In Figure 4c, the two conjunctions merged and stopped moving. Since on both sides of the united conjunction area, *A* has been formed, no new conjunction can emanate from this stripe. The angles within the pattern are dominated by 90º indicating that conjunctions stop rapid movement when they have reached directions parallel to the hillock orientation. Therefore, the stripe-pattern matches the orientation of the hillocks within the respective layer. The discrepancy between the orientation of the stripes and the hillocks in Figure 4c is caused by the different hillock orientation in successive layers (Aldushin *et al.*, 2004).

As the velocity of transformation $P \rightarrow T \rightarrow H$ at spreading hillocks depends on the pH of the solution so does the velocity of the rapidly moving conjunctions. However, the velocity of moving conjunctions is approximately five to eight times higher than the velocity of hillock spreading. As shown in Figure 5, the rate of moving conjunctions increases from ~15 nm/min at pH 3 to ~150 nm/min at pH 1.5. The data in Figure 5 are based on the highest rates obtained during the course of conjunction movement. The movement of conjunctions towards the final (enveloping) position is often hampered and temporarily pinned (*cf.* the zigzag shape of the conjunction in Figure 3c) causing the rates to vary strongly. Therefore only maximum values reflect the uninfluenced movement of conjunctions. Also, as shown in Figure 2, in some cases area *T* is permanently attached to the main hillock (area *H*) and does not separate and move at all (see also Figure 6).

The solution flowing through the fluid cell of the microscope can be exchanged *in situ*. A replacement of low-pH solutions by high-pH solutions significantly changes the reactions taking place on the apophyllite (001) surface. Increasing the pH to 9–12 causes existing hillocks, conjunctions, and the areas through which the conjunctions have passed (area *A*) to decompose within seconds. However, the pristine surface (area *P*) remains stable within the time frame of experiments. Figure 6a–d shows the apophyllite (001) surface at

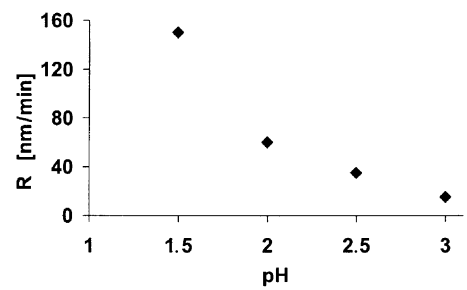

Figure 5. Maximum observed rate of conjunction movement *vs.* pH of solution.

https://doi.org/10.1346/CCMN.2004.0520404 Published online by Cambridge University Press

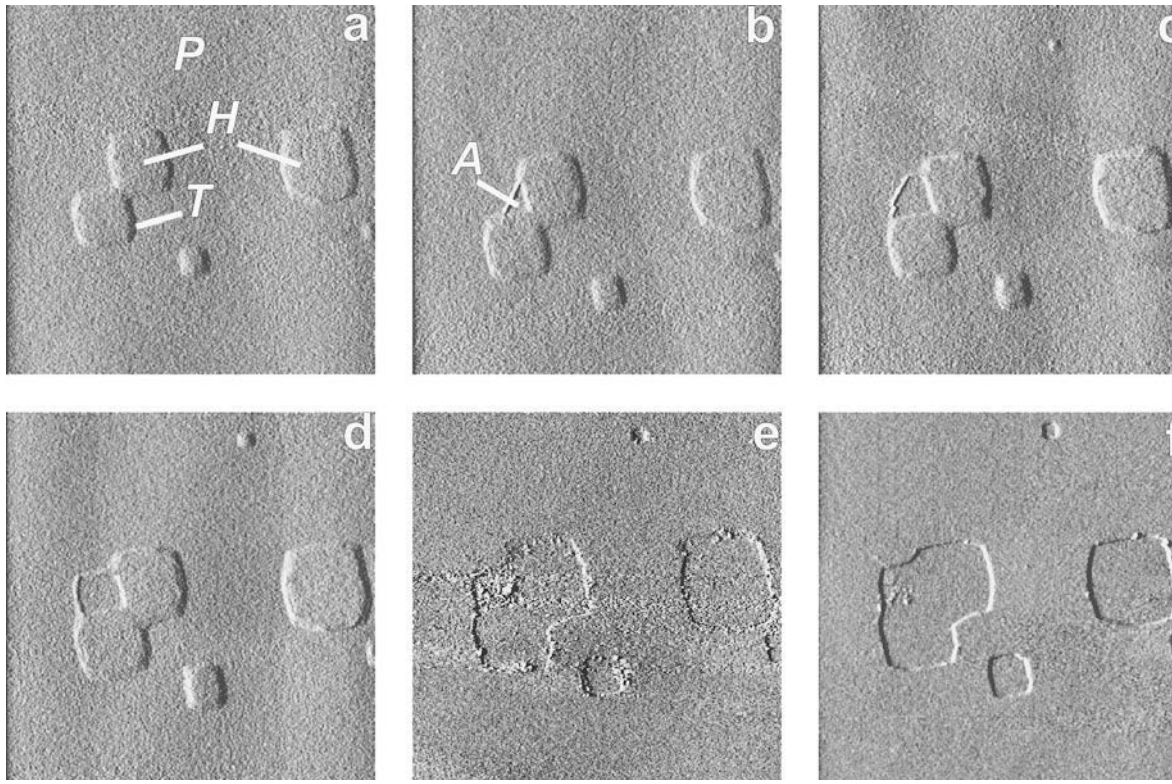

Figure 6. *In situ* exchange of solution – low pH → high pH (image acquisition for parts b, c, d, e and f at 3, 7, 14, 20 and 24 min after part a, respectively). (a–d) Low pH: two merging hillocks and development of the conjunction. Note that only in the inner corner to the upper left is a conjunction formed, whereas in the opposite corner the formation of a conjunction is impeded by area *T* being pinned to the mature hillock; (e–f) *in situ* exchange of the solution (pH 2.5 → pH 10): hillocks, conjunction, and area *A* decompose within seconds, leaving behind an inverse morphology. Scan field 2 μm × 2 μm.

low pH with two merging hillocks at the left side of the images. In the upper inner corner of the hillocks, area *T* separates and forms a conjunction (in the other corner area *T* is clearly pinned to the mature hillock). After the exchange of solution to high pH, the surface layer in areas *T*, *H* and *A* is decomposed leaving behind a negative morphology of all the areas that have been subject to alteration by interaction with acidic aqueous solution (Figure 6e). It is important to note that the decomposition of area *A* along with area *T* and *H* clearly shows that area *A* is not behaving like the pristine area *P* and therefore is clearly altered by the rapidly passing conjunction. However, as shown by the still visible remains of area *A* in Figure 6f, area *A* is more stable than *T* and *H*.

X-ray photoelectron spectroscopy (XPS)

The (001) surfaces of a freshly cleaved apophyllite crystal and of crystals immersed into acidic solution were examined by XPS. The resulting survey spectra are shown in Figure 7. The acidic solution causes a significant depletion of K^+, Ca^{2+} and F^-. Examining the relative peak intensities allows us to quantify the change in the chemical composition of the topmost layers of the apophyllite (001) surface relative to the untreated sample. The data, which are deduced from detailed measurements in the particular regions of interest are shown in Table 1 (for calculations Si 2*p*, K 2*p*, Ca 2*p* and F 1*s* peaks were used). Comparing the cation concentrations, Table 1 shows that the depletion of Ca^{2+} is significantly slower than the depletion of K^+. After treatment in pH 2.5 for 5 h, the concentration of Ca in the topmost layer decreases to ~4.7% (with respect to the pristine Ca concentration), whereas the concentration of K falls below the detection limit. By comparison, RBS depth profile analysis (Aldushin *et al.*, 2004) revealed that after a treatment of apophyllite samples in pH 2 solution for 10 h, the concentration of Ca + K decreases to ~18% at the surface. The lower cation concentration measured by XPS can be explained

Table 1. XPS analysis of the (001) surface of apophyllite treated in pH 2.5 solution.

	$C_{treated}/C_{untreated}$ [%]		
	1 h	3 h	5 h
Ca	19.8(8)	12.4(6)	4.7(3)
K	10.6(4)	8.5(4)	< 0.3
F	12.1(5)	7.5(4)	< 0.3

https://doi.org/10.1346/CCMN.2004.0520404 Published online by Cambridge University Press

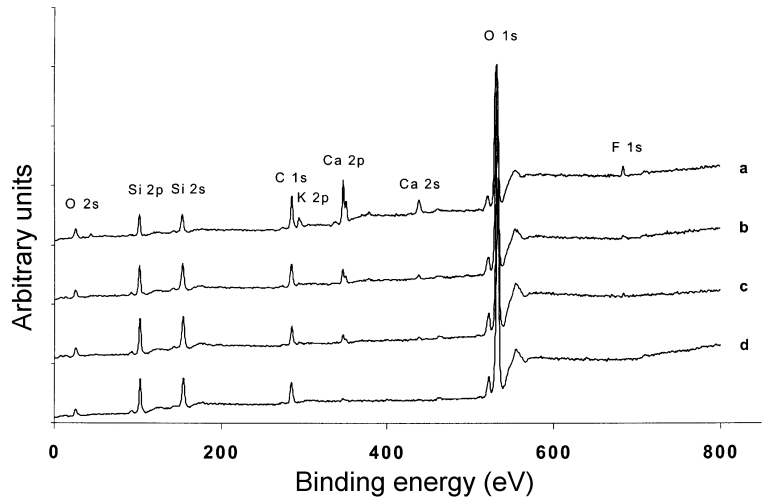

Figure 7. XPS spectra of the near-surface region on the (001) surface of apophyllite: (a) freshly cleaved surface; (b) sample immersed in pH 2.5 solution at room temperature for 1 h, (c) 3 h and (d) 5 h.

by the different sensitivities of the methods: for RBS the depth of information is ~10–15 nm, whereas XPS analyzes the chemical composition of minerals within the topmost 1–2 nm.

Nuclear magnetic resonance spectroscopy (NMR)

^{1}H MAS NMR spectra. The ^{1}H MAS NMR spectrum of untreated apophyllite in Figure 8a shows a single signal at 6.1 ppm and an extensive rotational side-band pattern which implies a strong homonuclear dipolar interaction for the ^{1}H nucleus. The signal can be assigned to water which is located in the octahedral sheets of the apophyllite (Yesinowski *et al.*, 1988; Fechtelkord *et al.*, 2003). Due to the small intermolecular distance of the water molecules a strong homonuclear dipolar interaction between the water molecule protons arises.

The acid-treated apophyllite shows a shift of the ^{1}H signal from 6.1 ppm to 5.2 ppm with decreasing pH value as shown in Figure 8. Moreover, the resulting linewidth decreases and the intensity of the sidebands gets lower. However, the sidebands did not change in lineshape. This can be interpreted in such a way that the original water signal is superimposed by a new narrow signal which gets stronger in intensity with decreasing pH value but shows nearly no sideband intensity. The signal can be assigned to silanol groups ($\equiv$Si-OH); the protons of these groups have no direct dipolar interaction and thus no sideband intensity. Additionally, in contrast to water, there is no hydrogen bonding to other OH groups causing a narrower signal.

^{29}Si MAS NMR and {^{1}H} ^{29}Si CPMAS NMR. The ^{29}Si MAS NMR spectrum of untreated apophyllite in Figure 9a shows a single ^{29}Si MAS NMR signal at −92.9 ppm caused by [Si(OSi)$_3$O$^-$] groups (SiO$_4$-groups with three bridging and one terminal oxygen). After the acid treatment three additional signals appear at −99.0, −101.7 and −103.4 ppm (Figure 9b). The three signals can be assigned to three different protonated silicon sites [Si(OSi)$_3$OH] (the terminal oxygen is protonated) with different tetrahedral bonding angles. This interpretation is supported by {^{1}H} ^{29}Si CPMAS NMR experiments

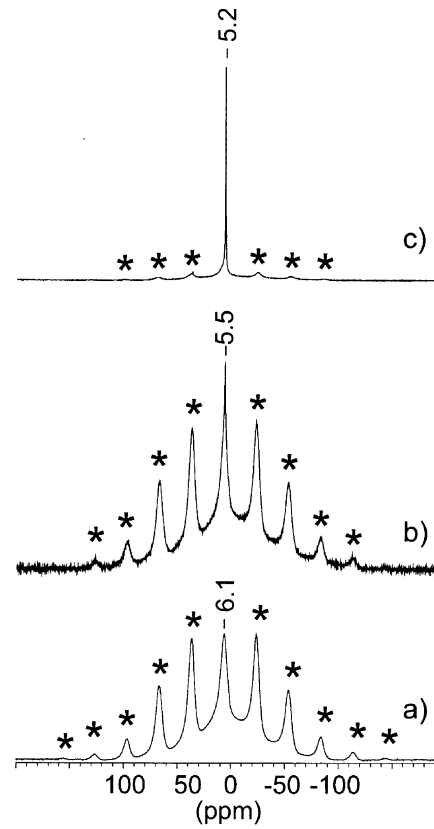

Figure 8. ^{1}H MAS NMR spectra of (a) untreated apophyllite, (b) treated at pH 2.5 for 1 h and (c) at pH 1.0 for 1 h. Asterisks mark spinning sidebands.

https://doi.org/10.1346/CCMN.2004.0520404 Published online by Cambridge University Press

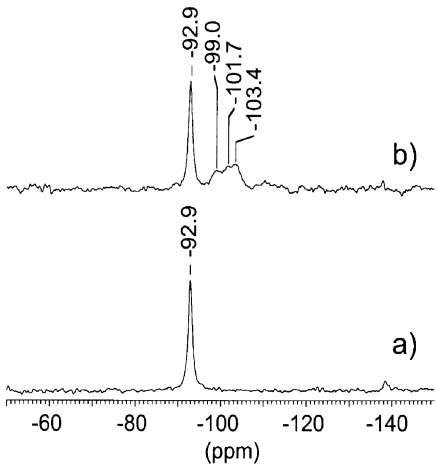

Figure 9. ^{29}Si MAS NMR spectra of (a) untreated apophyllite, and (b) treated at pH 1 for 1 h.

with varying contact times as shown in Figure 10. For a short contact time of 250 μs (Figure 10a), the three new components show a strong relative increase in signal intensity compared to the original apophyllite signal. With short contact times only those protons which are a short distance from Si sites (*i.e.* silanol protons) can transfer magnetization. Therefore, the signal increase can be considered as clear proof that these three signals are caused by silanol groups. With increasing contact time (Figure 10b,c), the signals at −98.9 and −101.2 ppm increase in relative intensity, showing that in this case also, close-by water molecules transfer magnetization. The intensity distribution at large contact times indicates that the signal at −103.0 ppm refers to the smallest amount of water molecules in the neighborhood. According to the ^{29}Si MAS NMR spectrum (Figure 9b), the most frequent silanol groups are those with the smallest amount of water in their vicinity.

After prolonged acidic treatment of the apophyllite sample (11 h in pH 1.6 solution), the ^{29}Si MAS NMR spectrum additionally exhibits a broad signal with a maximum at −111.0 ppm. This signal indicates $Si(OSi)_4$-type silica with varying bonding parameters comparable to poorly crystalline or even amorphous silica. In $\{^1H\}$ ^{29}Si CPMAS NMR experiments, this $Si(OSi)_4$-type signal is completely absent, indicating that this signal is not related to silanol groups. It is important to note further, that a signal of $[Si(OSi)_2(OH)_2]$ groups forming due to protonation of silicate tetrahedra at sheets edges was too weak to be detected by NMR.

DISCUSSION

The formation of hillocks nucleate at defect sites or steps on the apophyllite surface. At these positions, H_3O^+ molecules start to penetrate into the interlayer region and trigger an ion-replacement reaction. The reaction proceeds by spreading hillocks with straight

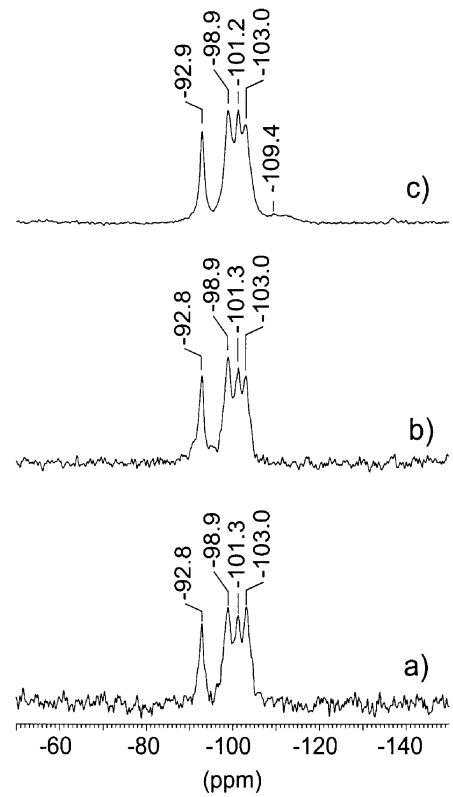

Figure 10. $\{^1H\}$ ^{29}Si CPMAS MAS NMR spectra of apophyllite treated at pH 1 for 1 h with contact times of (a) 250 μs, (b) 1 ms and (c) 3 ms.

steps. Therefore, alteration of the apophyllite (001) surface in acidic solution can be described by an ion-replacement reaction causing a protonated and cation-depleted residue (Aldushin *et al.*, 2004). However, the AFM experiments presented here show that this replacement reaction takes place in two or three successive stages that cause different morphological patterns. Thus, it can be inferred that the overall replacement reaction consists of a dual-step or triple-step process. The dual-step process is represented by the transformation of the pristine surface (area *P*) to area *T* and by the successive transformation of area *T* to the mature hillock (area *H*). The triple-step process comprises the transformations $P \rightarrow T \rightarrow A \rightarrow H$. Each of these four transformations ($P \rightarrow T$, $T \rightarrow H$, $T \rightarrow A$, $A \rightarrow H$) has distinct properties and, therefore, corresponds to a separate reaction.

The NMR and XPS experiments reveal the mechanism of reaction as a protonation of the terminal apex-position of the silicate tetrahedra forming silanol groups and causing removal of interlayer cations. The NMR results further show that three different protonation sites develop in apophyllite crystals in acidic solution. The three types of $\equiv O_3SiOH$-groups show differences in their amount of close-by hydrogen and structural differences, which are probably not related to the crystal structure itself due to equivalence of the structural units

https://doi.org/10.1346/CCMN.2004.0520404 Published online by Cambridge University Press

in apophyllite. The AFM experiments show that the formation of mature hillocks (*i.e.* the formation of maximum protonated silicate layers and fully cation-depleted interlayers – area *H*) takes places discontinuously in up to three transformation steps. This discontinuity and the fact that all three transformations are proton-promoted make it reasonable to assume that the transformations are associated with distinct protonation steps and types of silanol groups. If a mixture of all three protonation types was taking place initially, a continuous morphological transformation of the pristine surface to the mature hillocks would be expected.

Transformation $P \rightarrow T$

Since protonation via H_3O^+ implies the uptake of three hydrogen atoms in total, silanol groups with the smallest amount of close-by hydrogen can be expected to be found in an early stage of apophyllite protonation. Therefore, the type of protonation taking place in the initial transformation process $P \rightarrow T$ possibly causes the silanol group giving rise to the ^{29}Si MAS NMR signal at −103.0 ppm (*i.e.* the signal associated with the smallest amount of close-by hydrogen). The ^{29}Si MAS NMR signals of the other two silanol groups indicate larger amounts of close-by hydrogen and thus are more likely associated to silanol groups formed by subsequent transformations, as more water molecules diffuse into the interlayer space. The XPS results show a preferential release of K^+ compared to Ca^{2+}. Therefore, it is reasonable to assume that the release of K^+ is rather part of the initial transformation $P \rightarrow T$ than part of subsequent transformations.

When terraces coalesce (area *T*), *i.e.* when the transformation fronts $P \rightarrow T$ of two hillocks meet (Figure 3), the reaction rate increases considerably until the front reaches the position marked by the shape of an enveloping hillock. The rapid $P \rightarrow T$ transformation also takes place at steps which are not directed parallel to the according hillock orientation (Figure 4). This behavior has a remarkable likeness to the behavior of straight steps at coalescing etch pits during calcite and magnesite dissolution (Jordan and Rammensee, 1998; Jordan *et al.*, 2001). At these coalescing pits, jagged and unbounded steps are generated which retreat at high rates until the pit has reached the shape of an enveloping pit with straight steps. The requirements for straight shape steps can be described by the terrace-ledge-kink-model (Liang *et al.*, 1996; Jordan *et al.*, 2001). At straight steps, the removal of units parallel to the step direction (*i.e.* removal at kinks) is much faster than the removal of units perpendicular to the step direction (*i.e.* nucleation of kink sites or 'double kink sites'). At jagged steps formed by coalescing straight steps, material can dissolve without the slow nucleation of double-kink sites. Therefore, the step-retreat rate increases and the steps become jagged or zigzag shaped. The retreat rate of jagged steps is not hampered by the slow nucleation rate of double-kink sites. Therefore, coalescing jagged steps cannot generate steps with an enhanced retreat rate. The remarkable likeness of the behavior of transformation reaction $P \rightarrow T$ on the (001) surface of apophyllite to carbonate dissolution suggests analogy. Since protonation of the silicate apices in apophyllite is the process corresponding to the removal of material at carbonate steps, it can be inferred that protonation parallel to the direction of the reaction front is much faster than perpendicular. Also, impurities or defects suspected to cause pinning of step retreat on calcite (Jordan & Rammensee, 1998) may be also responsible for the pinning of the rapid $P \rightarrow T$ transformation.

Transformation $T \rightarrow A$

The transformation $T \rightarrow A$ takes place exclusively subsequent to the rapid $P \rightarrow T$ transformation. In analogy to carbonate dissolution, the jagged transformation front $T \rightarrow H$ was never observed to move as rapidly as the straight $P \rightarrow T$ transformation front. Therefore, in the case of rapid $P \rightarrow T$ transformation, the width of area *T* should increase noticeably, as the $T \rightarrow$ H transformation cannot attain the same rate. This increased width of area *T* would correspond to a longer residence time of a certain location in the protonated state *T*. However, according to our observations, the residence time of the protonation state *T* induced by the rapid $P \rightarrow T$ transformation does not increase, *i.e.* the terrace always keeps roughly the same width. Since the $T \rightarrow H$ transformation does not take place in time, a transformation into state *A* follows. The state *A* is characterized morphologically by a decreased height (in comparison with state *T*), approximately at the level of the pristine surface. In contrast to state *T*, state *A* exhibits a surprisingly high stability: it even has better resistance against the transformation into the state of maximum protonation than the pristine surface, *i.e.* $A \rightarrow H$ is slower than $P \rightarrow T \rightarrow H$.

Further assessments of state *A* can be made by performing an *in situ* exchange of the low-pH solution for solution at pH > 9. In the high-pH solution, not only the hillock areas *T* and *H* decompose quickly, but also area *A*. The pristine surface (area *P)* remains stable in high-pH solutions within the time scale of experiments. This clearly shows that area *A* is altered with respect to the pristine surface. Also, the sensitivity of state *A* to high-pH solutions makes it reasonable to assume that state *A* still has protonated silicate groups despite the strong decrease in surface height. However, there is little information whether the transformation $T \rightarrow A$ involves a further protonation, *i.e.* an increased density of protonated silicate apices within the apophyllite interlayer. Even if no further protonation was associated with the $T \rightarrow A$ transformation, the structural modifications induced by $T \rightarrow A$ probably cause modifications of the Si-OH bonding parameters and of the amount of close-by hydrogen. Considering surface silanol groups, even

https://doi.org/10.1346/CCMN.2004.0520404 Published online by Cambridge University Press

slight structural modifications have been shown to exert considerable influence on bonding parameters (Bickmore *et al.*, 2003, 2004). Thus, the transformation $T \rightarrow A$ might be responsible for the formation of the second type of silanol groups detected by NMR.

Transformation $T \rightarrow H$ and $A \rightarrow H$, amorphous structures

The final transformation into the mature hillock (state *H*) can take place either from the highly stable state *A* or from terrace state *T*. Both transformations are proton-promoted reactions, but the transformation rates are noticeably different. After the transformation fronts $T \rightarrow H$ or $A \rightarrow H$ have passed on the surface, further changes in surface morphology or layer height cannot be detected by AFM. Since state *H* is highly sensitive to the forces exerted by the scanning tip, it does not bear prolonged probing and, therefore, an assessment of a progressive alteration of the structure beyond state *H* is not possible. In this respect, NMR analysis points towards a progressive structural degradation manifested in the broad signal around −111.0 ppm after a prolonged acidic treatment (11 h at pH 1.6) of the apophyllite sample. This structural degradation is in accordance with the results reported by Lagaly and Matouschek (1980).

CONCLUSIONS

Acidic treatment of layered silicates causes the depletion of interlayer cations and the formation of a hydrated porous or layered silica residue. In the present study, the combined AFM, NMR and XPS approach provides detailed information on the mechanism of this process. On apophyllite surfaces, depletion of interlayer cations is initiated and accompanied by protonation of the terminal apices of silicate tetrahedra. The NMR results revealed that the protonation sites are not equivalent, although they are of the same type, *i.e.* $Si(OSi)_3(OH)$. According to NMR data presented in other studies, for many clay minerals only one uniform $[Si(OSi)_3OH]$ protonation site has been reported (*e.g.* Kaviratna and Pinnavaia, 1994; Kosuge *et al.*, 1995; Komadel *et al.*, 1996; Aznar *et al.*, 1996; Okada *et al.*, 2002). In this respect, the product of apophyllite acidic treatment is different from those of other phyllosilicates, indicating that structural differences between sheet silicates play a key role in the mechanisms taking place due to acidic treatment. However, a computer modeling approach, which was successfully applied for solution and surface functional groups (*e.g.* Tossell and Sahai, 2000; Bickmore *et al.*, 2003, 2004) is desirable in order to obtain more detailed knowledge of the structure and mechanisms taking place within the apophyllite interlayers.

In the case of apophyllite, protonation takes place in a two- or three-step process. The protonation states differ significantly in their formation rate and stability. While in some cases the initial protonation can attain high rates, the rate of the subsequent rising of interlayer distance by a further protonation is constant. This rate difference along with the limited stability of the initially protonated state can cause the formation of an intermediate, metastable state that shows a remarkable stability against further protonation – even with respect to the pristine surface. As AFM shows the silicate layers peeling off the surface once the two- (three-) step protonation has been completed, NMR results indicate further advancing decomposition of the apophyllite structure in the bulk mineral.

ACKNOWLEDGMENTS

Financial support from the Deutsche Forschungsgemeinschaft is gratefully acknowledged. We also thank Randall T. Cygan, Barry R. Bickmore and an anonymous reviewer for helpful suggestions and comments on the manuscript.

REFERENCES

Aldushin, K., Jordan, G., Rammensee, W., Schmahl, W.W. and Becker, H.-W. (2004) Apophyllite (001) surface alteration in aqueous solutions studied by HAFM. *Geochimica et Cosmochimica Acta*, **68**, 217–226.

Astilleros, J.M., Pina, C.M., Fernandez-Diaz, L. and Putnis, A. (2002) Molecular-scale surface processes during the growth of calcite in the presence of manganese. *Geochimica et Cosmochimica Acta*, **66**, 3177–3189.

Aznar, A.J., Gutierrez, E., Diaz, P., Alvarez, A. and Poncelet, G. (1996) Silica from sepiolite: Preparation, textural properties, and use as support to catalysts. *Microporous Materials*, **6**, 105–114.

Bickmore, B.R., Bosbach, D., Hochella, Jr., M.F., Charlet, L. and Rufe, E. (2001) *In situ* atomic force microscopy study of hectorite and nontronite dissolution: Implications for phyllosilicate edge surface structures and dissolution mechanisms. *American Mineralogist*, **86**, 411–423.

Bickmore, B.R., Rosso, K.M., Nagy, K.L., Cygan, R.T. and Tadanier, C.J. (2003) *Ab initio* determination of edge surface structures for dioctahedral 2:1 phyllosilicates: Implications for acid-base reactivity. *Clays and Clay Minerals*, **51**, 359–371.

Bickmore, B.R., Tadanier, C.J., Rosso, K.M., Monn, W.D. and Eggett, L.D. (2004) Bond-valence methods for pK_a prediction: Critical reanalysis and a new approach. *Geochimica et Cosmochimica Acta*, **68**, 2025–2042.

Bosbach, D., Charlet, L., Bickmore, B. and Hochella, Jr., M.F., (2000) The dissolution of hectorite: In-situ, real-time observations using atomic force microscopy. *American Mineralogist*, **85**, 1209–1216.

Brandt, F., Bosbach, D., Krawczyk-Barsch, E., Arnold, T. and Bernhard, G. (2003) Chlorite dissolution in the acid pH-range: A combined microscopic and macroscopic approach. *Geochimica et Cosmochimica Acta*, **67**, 1451–1461.

Cave, L.C. (2002) Apophyllite weathering and the aqueous geochemistry of a Karoo breccia pipe. PhD thesis, Department of Geological Sciences, University of Cape Town, Republic of South Africa.

Colville, A.A., Anderson, C.P. and Black, P.M. (1971) Refinement of the crystal structure of apophyllite, I. X-ray diffraction and physical properties. *American Mineralogist*, **56**, 1222–1233.

Corma, A. and Perez-Periente, J. (1987) Surface acidity and

activity of modified sepiolite. *Clay Minerals*, **22**, 423–433.
Deuster, V., Schick, M., Kayser, T., Dabringhaus, H., Klapper, H. and Wandelt, K. (2003) Studies of the facetting of the polished (100) face of CaF_2. *Journal of Crystal Growth*, **250**, 313–323.
Duckworth, O.W. and Martin, S.T. (2003) Connections between surface complexation and geometric models of mineral dissolution investigated for rhodochrosite. *Geochimica et Cosmochimica Acta*, **67**, 1787–1801.
Fechtelkord, M., Behrens, B., Holtz, F., Fyfe, C.A., Groat, L.A. and Raudsepp, M. (2003) Influence of F content on the composition of Al-rich synthetic phlogopite: Part I. New information on structure and phase-formation from ^{29}Si, ^{1}H, and ^{19}F MAS NMR spectroscopies. *American Mineralogist*, **88**, 47–53.
Frondel, C. (1979) Crystalline silica hydrates from leached silicates. *American Mineralogist*, **64**, 799–804.
Higgins, S.R., Jordan, G. and Eggleston, C.M. (2002) Dissolution kinetics of magnesite in acidic aqueous solution: a hydrothermal atomic force microscopy study assessing step kinetics and dissolution flux. *Geochimica et Cosmochimica Acta*, **66**, 3201–3210.
Jordan, G. and Rammensee, W. (1998) Dissolution rates of calcite (10-14) obtained by scanning force microscopy: Microtopography-based dissolution kinetics on surfaces with anisotropic step velocities. *Geochimica et Cosmochimica Acta*, **62**, 941–947.
Jordan, G., Higgins, S.R., Eggleston, C.M., Swapp, S.M., Janney, D.E. and Knauss, K.G. (1999) Acidic dissolution of plagioclase. *In-situ* observations by hydrothermal atomic force microscopy. *Geochimica et Cosmochimica Acta*, **63**, 3183–3191.
Jordan, G., Higgins, S.R., Eggleston, C.M., Knauss, K.G. and Schmahl, W.W. (2001) Dissolution kinetics of magnesite in acidic aqueous solution, a hydrothermal atomic force microscopy (HAFM) study: Step orientation and kink dynamics. *Geochimica et Cosmochimica Acta*, **65**, 4257–4266.
Kaviratna, H. and Pinnavaia, T.J. (1994) Acid hydrolysis of octahedral Mg^{2+} sites in 2:1 layered silicates: an assessment of edge attack and gallery access mechanisms. *Clays and Clay Minerals*, **42**, 717–723.
Komadel, P., Madejová, J., Janek, M., Gates, W.P., Kirkpatrick, R.J. and Stucki J.W. (1996) Dissolution of hectorite in inorganic acids. *Clays and Clay Minerals*, **44**, 228–236.
Kosuge, K., Shimada, K. and Tsunashima, A. (1995) Micropore formation by acid treatment of antigorite. *Chemical Materials*, **7**, 2241–2246.
Lagaly, G. and Matouschek, R. (1980) The crystalline silicic acids from apophyllite, carletonite and gillespite. *Neues Jahrbuch für Mineralogie Abhandlungen*, **138**, 81–93.
Lagaly, G., Beneke, K. and Weiss, A. (1975) Magadiite and H-Magadiite: II. H-Magadiite and its intercalation compounds. *American Mineralogist*, **60**, 650–658.
Liang, Y., Baer, D.R., McCoy, J.M., Amonette, J.E. and LaFemina, J.P. (1996) Dissolution kinetics at the calcite-water interface. *Geochimica et Cosmochimica Acta*, **60**, 4883–4887.
Liu, C., Li, X.Y., Xu, F.L. and Huang, P.M. (2003) Atomic force microscopy of soil inorganic colloids. *Soil Science and Plant Nutrition*, **49**, 17–23.
Nagy, K.L., Blum, A.E. and Lasaga, A.C. (1991) Dissolution and precipitation of kaolinite at 80ºC and pH 3: The dependence on solution saturation state. *American Journal of Science*, **291**, 649–686.
Okada, K., Nakazawa, N., Kameshima, Y., Yasumori, A., Temuujin, J., MacKenzie, K.J.D. and Smith, M.E. (2002) Preparation and porous properties of materials prepared by selective leaching of phlogopite. *Clays and Clay Minerals*, **50**, 624–632.
Pabst, A. (1958) The crystal structure of leached gillespite, a sheet silicate. *American Mineralogist*, **43**, 970–980.
Peskleway, C.D., Henderson, G.S. and Wicks, F.J. (2003) Dissolution of gibbsite: Direct observations using fluid cell atomic force microscopy. *American Mineralogist*, **88**, 18–26.
Ravichandran, J. and Sivasankar, B. (1997) Properties and catalytic activity of acid-modified montmorillonite and vermiculite. *Clays and Clay Minerals*, **45**, 854–858.
Rodriguez, M.A.V., Gonzalez, J.D.L. and Munoz, M.A.B. (1994) Acid activation of a Spanish sepiolite: physicochemical characterization, free silica content and surface area of products obtained. *Clay Minerals*, **29**, 361–367.
Saito, Y., Motohashi, T., Hayashi, S., Yasumori, A. and Okada, K. (1997) High thermal resistance of gamma-Al_2O_3 prepared by the selective leaching of calcined kaolin minerals. *Journal of Materials Chemistry*, **7**, 1615–1621.
Shiraki, R., Rock, P.A. and Casey, W.H. (2000) Dissolution kinetics of calcite in 0.1 M NaCl solution at room temperature: An atomic force microscopic (AFM) study. *Aquatic Geochemistry*, **6**, 87–108.
Sogo, Y., Iizuka, F. and Yamazaki, A. (1998) Preparation and properties of layered silica and layered alumino-silica hydrate from natural apophyllite. *Journal of the Ceramic Society of Japan*, **106**, 160–168.
Temuujin, J., Burmaa, G., Amgalan, J., Okada, K., Jadambaa, T. and MacKenzie K.J.D. (2001) Preparation of porous silica from mechanically activated kaolinite. *Journal of Porous Materials*, **8**, 233–238.
Teng, H.H., Fenter, P., Cheng, L.W. and Sturchio N.C. (2001) Resolving orthoclase dissolution processes with atomic force microscopy and X-ray reflectivity. *Geochimica et Cosmochimica Acta*, **65**, 3459–3474.
Tossell, J.A. and Sahai N. (2000) Calculating the acidity of silanols and related oxyacids in aqueous solution. *Geochimica et Cosmochimica Acta*, **64**, 4097–4113.
Walther, J.V. (1996) Relation between rates of aluminosilicate mineral dissolution, pH, temperature, and surface charge. *American Journal of Science*, **296**, 693–728.
Wieland, E. and Stumm, W. (1992) Dissolution kinetics of kaolinite in acidic aqueous solutions at 25ºC. *Geochimica et Cosmochimica Acta*, **56**, 3339–3355.
Yesinowski, J.P., Eckert, H. and Rossman, G.R. (1988) Characterization of hydrous species in minerals by high-speed ^{1}H MAS-NMR. *Journal of the American Chemical Society*, **110**, 1367–1375.

(*Received 15 September 2003; revised 1 March 2004; Ms. 833; A.E. Randall T. Cygan*)